Optimal Self-Tuning Control for Data-Centers' 48V-12V ZCS-STC

Guy Sovik, *Student Member*, *IEEE*, Tom Urkin, *Student Member*, *IEEE*, Erez Erzol Masandilov, *Student Member*, *IEEE*, and Mor Mordechai Peretz, *Member*, *IEEE*

The Center for Power Electronics and Mixed-Signal IC, Department of Electrical and Computer Engineering
Ben-Gurion University of the Negev, P.O. Box 653, Beer-Sheva, 8410501 Israel
sovik@post.bgu.ac.il, tomur@post.bgu.ac.il, masander@post.bgu.ac.il, morp@bgu.ac.il
http://www.ee.bgu.ac.il/~pemic

***Abstract* – This paper presents a zero-current-switching (ZCS) control method with self-tuning capabilities employed on a 4-to-1 switched-tank converter (STC) for Google's and associated OCP standard data-centers. The control scheme ensures ZCS operation of each of the STC's resonant tanks individually, regardless of components mismatch, and adjusts the switching period upon variations of the components' values. The switching-state of the STC's resonators is evaluated at the turn-off instance by dedicated zero-current-detection indicator. Two approaches have been developed for the sensor's data acquisition, accounting for the inherent delay between the digital-controller gating command and the actual turn-off of the switches. The operation of the control has been validated experimentally on 650W 4-to-1 STC with PCB area of 5cmX2cmX0.6cm, demonstrating exceptional self-tuning capabilities over the entire load range and for various component mismatch scenarios. Peak efficiency of 98.6% is achieved at 200W.**

Keywords – self-tuned control, switched capacitor converter, switched tank converter, soft switching, zero-current-switching (ZCS).

I. Introduction

Switched-Capacitor Converters (SCC) which have been rigorously explored over the last two decades [1]-[11] have established a dominant role in power management in data-centers and other cloud computing related applications. In light of the acceleration of the standardization of the power delivery structure that has been heavily affected by the trend-leading open-computing-project consortium (OCP) [12], the necessity to step the 48V rail down to 12V with extremely high efficiency and very high power density has established an application stand point at which SCC technology and its derivatives is highly superior over the inductor-based alternatives.

The OCP standardization broadly directs toward power delivery architecture that divides a processor PCB into two main power sections. The first section is the processor power path which includes the main processing unit and the DDR. There, the 48V rail is stepped-down to 12V level (i.e. 4-to-1 non-regulated conversion ratio) and the tightly regulated 1.xV required at the high-performance ICs is provided by VRM units, typically realized by multiphase buck converters. The second power path is the point-of-load (PoL) line where the main rail is stepped down to a voltage level limited at 14V, then the voltage is manipulated to various levels (5v, 3.3V, etc.) by PoL converters. Since the main voltage level may exceed up to 60V, a 4-to-1 conversion ratio may result in a higher voltage than it is allowed at the PoL inputs. Therefore, either higher conversion ratio or a 12V regulated solution are employed.

Power density and conversion efficiency are of key importance in data-centers applications (to maximize the amount of computing power per volume). This translates onto extremely strict conversion performance requirements at the 48V-to-12V level so that it would not further deteriorate the attractiveness of the overall solution. Since this application calls for a fixed conversion ratio, SCC technology renders a very attractive candidate. At medium power levels, SCCs and their derivatives have widely demonstrated peak efficiency over 98% [13]-[15]. Results of resonant SCC (RSCC) based power converters for data-centers applications, demonstrating peak efficiency of 98.5% around 200W have been recently presented [16]-[18].

The superiority of SCC and RSCC to produce very high efficiencies at fixed conversion ratios that match their no-load target voltages has been widely studied in the literature, for example in [19]-[24]. The recent bursts in improvement of semiconductors for intermediate voltage levels have enabled to significantly lower the equivalent resistance (R_{eq}) of these converters, resulting in very attractive efficiency characteristics at medium power levels. This change also shifted the loss breakdown of the converters in favor of the soft-switched (resonant) versions of SCCs since the contribution of the rms current to the overall losses is made smaller than the contribution of the switching actions. As a consequence, the switching frequency can be increased, reducing the size requirements of the passive components, further improving the power density.

Various switched-tank converter (STC) topologies, which are derived from the Dickson SCC [25], have been introduced in [16]. In a 4:1 STC, employed for 48V to 12V intermediate bus conversion in data-centers, two flying capacitors are substituted by *LC* resonators to facilitate soft-switching. To fully utilize the benefits of soft-switching, the conduction time

978-1-7281-4829-8/20/$31.00 ©2020 IEEE

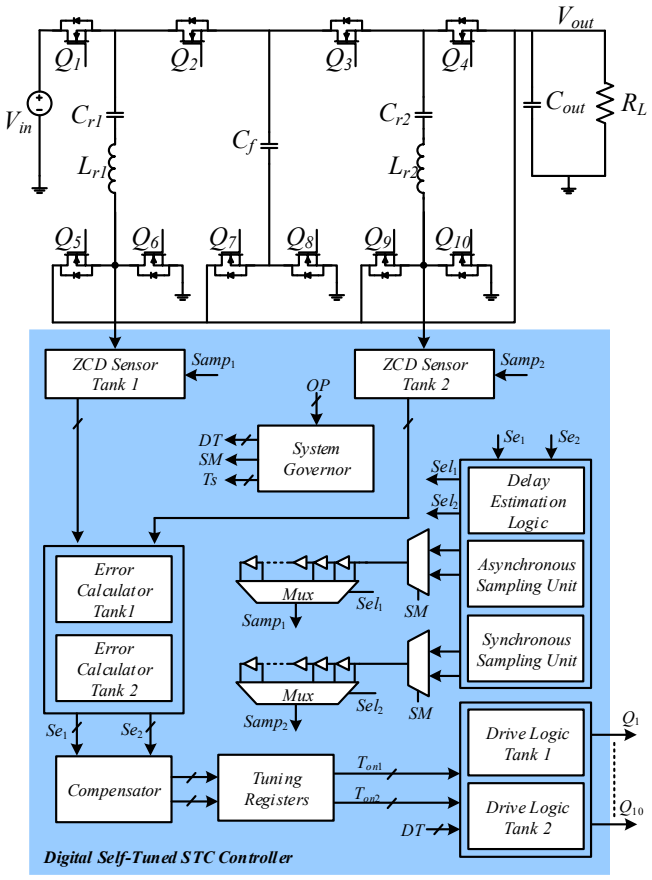

Fig. 1. Simplified schematic diagram of a 4:1 STC with digital self-tuning controller.

of each switching state should match exactly half of the resonant period. The exact characteristics of the resonators are considered unknown due to components tolerances and vary due to temperature- and aging-related drifts, physical layout of the design, loading conditions and components' stresses which limit the ability to achieve soft-switching with fixed conduction time. Development of a control method for the STC along with zero-current-detection (ZCD) sensors, to identify the resonant period of each resonator on-the-fly, converge to the optimal switching time, and compensate for variations of the resonant characteristics has been pursued in this study.

The objective of this study is to introduce a self-tuned control method to efficiently operate a switched-tank converter for Google's and OCP standard data-centers, and assure soft-switching operation under wide range of operating conditions and components variations, without sacrificing accuracy. Fig. 1 shows simplified schematic diagram of a 4:1 STC with the main building blocks of the control method realization. It is a further objective of this study to present a reliable and cost-effective zero-current-detect sensor for the STC that can be easily integrated in a digital control scheme.

The rest of the paper is organized as follows: Section II details the principle of operation of a 4:1 STC, covering full circuit details, with matched and mismatched resonators. Section III describes the ZCD sensing scheme and self-tuned zero-current switching control. Simulation results and

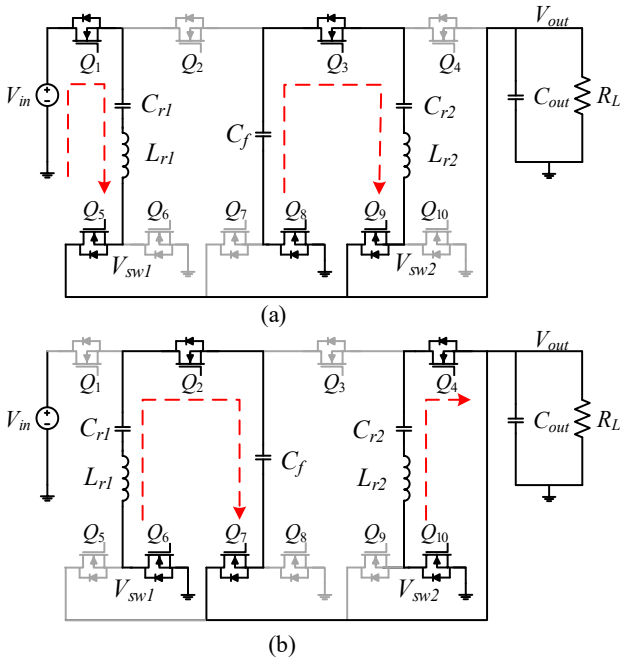

Fig. 2. Equivalent circuits of the 4:1 STC. (a) Charging-state. (b) Discharging state.

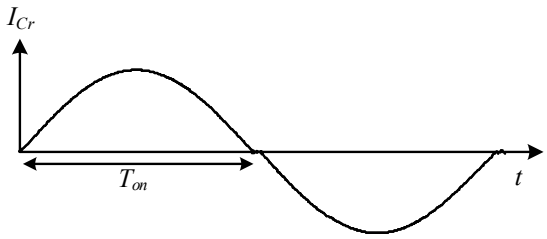

Fig. 3. Resonator's steady-state current waveform.

experimental validation on a 4:1 STC prototype are provided in Section IV. Section V concludes the paper.

II. Switched-Tank Converter

A. Principle of Operation

The STC is composed of 2 building blocks: flying capacitor and switched-resonant-tank, which comprises a capacitor and an inductor, as can be observed in Fig. 1. The STC's operation can be divided into two states – charging or discharging of the resonators as shown in Fig. 2, with a short dead-time period between them. The resonators are either charged from the input and flying capacitor or discharged into the flying capacitor and output. In each state the flying capacitor is connected in series to a resonant tank, thus guaranteeing soft-charging for all capacitors in the system. Furthermore, soft-switching can be achieved due to the resonant nature of the current in all switches.

In a 4:1 STC C_{r1}, C_f and C_{r2} hold DC values of $3V_{out}$, $2V_{out}$ and V_{out} respectively. All switches are situated between resonant, flying, input or output capacitors, resulting in clamped drain-source voltage of V_{out} or $2V_{out}$. This low voltage clamping enables the use of very-low $R_{ds\text{-}on}$, state-of-the-art switches to improve efficiency [26]-[27].

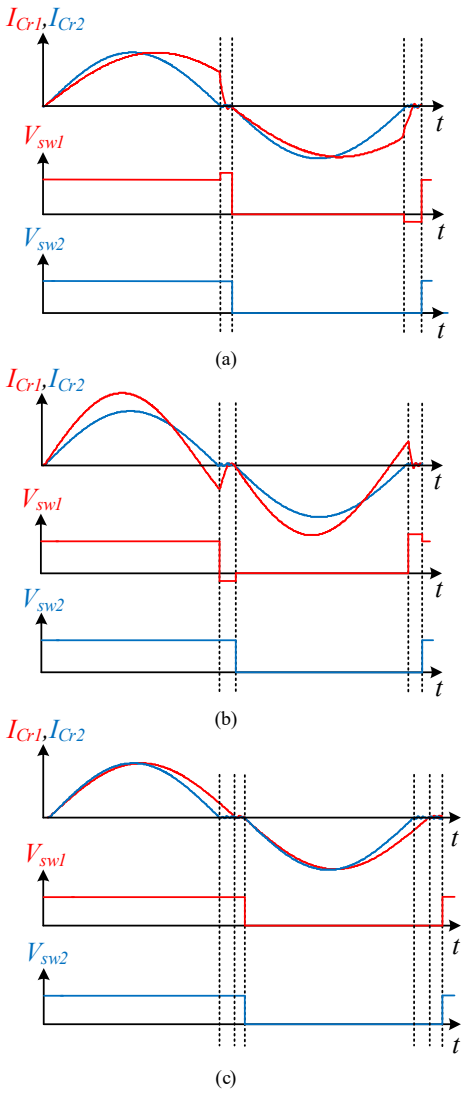

Fig. 4. Mismatched resonators steady-state current waveforms. (a) Early-switching of the first resonator. (b) Late-switching of the first resonator. (c) Tuned ZCS operation of both resonators.

Due to the low resistance in each current path, high quality-factor is maintained for all current-loops, hence:

$$Q = \frac{1}{R_{loop}}\sqrt{\frac{L_r}{C_r}} \gg 1, \tag{1}$$

where C_r and L_r are the resonant capacitor's and inductor's values, and R_{loop} is the sum of all parasitic resistances in the current's path. The DC current through each tank equals half of the output current and can be approximated as sinusoidal by neglecting the short dead-time period:

$$I_{C_r}(t) = \frac{\pi}{4} I_{out} \sin(2\pi f_r t) \quad ; \quad f_r = \frac{1}{2\pi\sqrt{L_r C_r}}, \tag{2}$$

where I_{Cr} is the resonator's current, I_{out} is the DC output current, and f_r is the resonance frequency. The flying capacitor is chosen such that it will not affect the resonant frequency ($C_f >> C_r$). By integrating (2) over the duration of the charging period, the amount of charge delivered to the load can be derived according to the following equation:

$$Q_{C_r} = \frac{1}{8 f_r} I_{out}[1 - \cos(2\pi f_r T_{on})]. \tag{3}$$

It can be seen from (3) that maximum charge is delivered per cycle when T_{on} equals half the resonant period and can be expressed as:

$$Q_{C_{r_{max}}} = \frac{1}{4 f_r} I_{out}. \tag{4}$$

Fig. 3 illustrates a typical current waveform of the resonant tanks for one steady-state cycle. It should be emphasized that the optimal T_{on} is half the resonant period. Any other on-time results not only in lower charge transfer rate but also in early- or late-switching, which introduces switching losses.

B. Operation with Non-Ideal Components and Indicator of ZCS

ZCS for all switches as well as obtaining the maximum charge transfer rate to the load is achieved when the duration of the charging-state equals half of the resonant period. Given that the resonant frequency depends on the STC's passive components, the switches' on-time can be calculated in advance. However, in practical systems the passive components tend to vary from their nominal values which may lead to non-ZCS operation. Furthermore, component variations result in mismatched resonant tanks with different resonant frequencies, which cannot be analytically derived. The steady-state performance of this topology highly depends on the ability to achieve ZCS in all resonators. Manual calibration of the on-times for each resonant tank is extremely time-consuming, and is not an approach viable for industrial integration. Moreover, it does not take into account components values' drifts due to aging or temperature [28]-[29].

The operation of a STC with mismatched resonant tanks ($C_{r1} \neq C_{r2}$, $L_{r1} \neq L_{r2}$) is illustrated in Fig. 4. Typical resonant current waveforms are shown in Fig. 4a-b where the switching of both tanks is based on the resonant frequency of the second tank (C_{r2}, L_{r2}) alone. Constant switching frequency results in non-ZCS operation of a single resonator as shown here, or of both in a more severe case. The reduced charge transfer rate to the load causes lower output voltage, as well as decreased efficiency due to the switching losses introduced by the residual currents of the resonators at the switching instance. Fig. 4c illustrates a case where the on-time of each tank is determined according to its resonant frequency, resulting in full ZCS operation. To allow constant switching frequency for both tanks, the switching period is calculated based on the following equation:

$$T_{SW} = 2T_{on\_max} + 2DT \quad ; \quad T_{on\_max} = \max\{T_1, T_2\}, \tag{5}$$

where DT is the applied dead-time and T_1, T_2 are the tuned on-times for full ZCS operation.

Tuning into ZCS can be obtained by evaluation of the currents at the switching instances followed by the required

modifications to the on-times of each tank. The most straightforward approach for zero-current-detection (ZCD) is current sensing. Shunt resistor, $R_{ds,on}$ sensing, SenseFET and current transformers [30]-[31] are all viable solutions, but require overdesign or additional protection circuitry, due to the high currents in the tanks (tens of Amps under full load conditions) and the actual low currents which are of interest at the switching moments. In this study, a different approach to obtain the currents' polarity at the switching instance has been implemented, while keeping a simple and cost-effective design.

Here, the voltages of the switching nodes (V_{SW1} and V_{SW2} in Fig. 2) at the end of the charging-state, i.e. the turn-off instance of Q_1 (Q_3) and Q_5 (Q_9) are used as indicators for early-, late-, or zero-current switching, as illustrated in Fig. 4a-c. In the case of early-switching of the first tank (Fig. 4a), the continuity of the resonant current forces the conduction of Q_5's body-diode, and V_{SW1} is clamped to $V_{out}+V_F$, where V_F is the forward voltage of the body-diode. In case the first tank operates with excessive on-time (late-switching), the resonant current's polarity reverses during the charging period and at the turn-off instance the node's voltage is clamped to $-V_F$, as shown in Fig. 4b. Only for the case of ZCS (Fig. 4c) the voltage of the switching node remains unchanged, therefore an indicator for early-, late-, or zero-current-switching is obtained.

III. ZCS Detection Circuit and Control Method

A. Sensing Circuit

As described earlier, the on-time of each resonant tank is modified to achieve ZCS based on the voltages at the bottom switching nodes (V_{SW1} and V_{SW2} in Fig. 2) which act as direct indicators to the polarity of the resonant current at the switching moment. Fig. 5 shows a two-comparator based ZCD sensor, employed in this study, which produces a 2-bit representation of the switching-node voltage. Two references are produced as a function of the output voltage, V_{th1} and V_{th2} in Fig. 5, which feed the upper and lower comparators negative inputs, respectively. This configuration acts as a small thermometric coder, translating the voltage to one of the following digital words: 2'*b*00, 2'*b*01 and 2'*b*11, which at the switching moment correlate to late-switching, zero-current-switching and early-switching, respectively. All possible ZCD sensor outputs are summarized in Table I.

The ZCD sensor's resistors are chosen according to the following expression:

$$\frac{R_C}{R_B+R_C+R_A} < \frac{R_2}{R_1+R_2} < \frac{R_B+R_C}{R_B+R_C+R_A}, \qquad (6)$$

where R_1 and R_2 determine the gain of the sensed switching node and R_A, R_B and R_C determine the reference window. Due to the drain-source capacitance of the power switches in practical systems, clamping to $-V_F$ is not guaranteed in case of light-load or low residual currents at the turn-off moment. Therefore, a small reference window around V_{Sensed} has been realized to ensure accurate tuning to ZCS under all conditions. The sensor tracks the output voltage and produces the references so that convergence to ZCS is guaranteed, regardless of the switching-state (i.e. early- or late-switching) upon start-up.

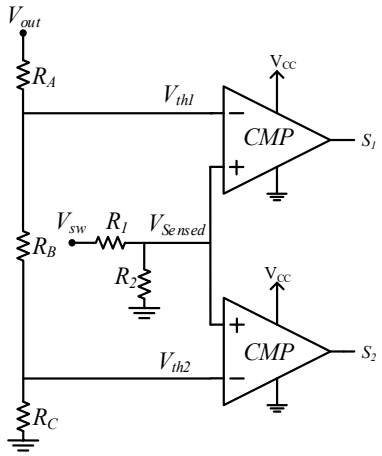

Fig. 5. Switching node voltage sensing circuit.

TABLE I – ZCD Sensor

Condition	S_1	S_2
$V_{Sensed} > V_{th1}$	1'*b*1	1'*b*1
$V_{Sensed} < V_{th2}$	1'*b*0	1'*b*0
$V_{th2} < V_{Sensed} < V_{th1}$	1'*b*0	1'*b*1

B. Auto-Tuned ZCS

Inherent delay between the generated gating signals in the controller and the actual conduction of the transistors is quite common for all switch-mode applications. This delay is generally unknown and may significantly vary as a function of the operating point or the passive components, driving circuitry and power transistors used. In addition, as in many realizations of ZCD sensors, indicator that has been employed (detailed earlier) produces usable information around the vicinity of the switching since it is based on reading the clamping diodes status. Therefore, sampling the ZCD sensors must be able to compensate, or at least consider this inherent delay so that an accurate status information is obtained, i.e. early or late switching. In this study, two approaches have been realized to acquire the information from the ZCD sensors while accounting for the above-mentioned delay.

The first approach, referred to as *synchronous sampling*, is based on continuous sampling of the ZCD sensors. During the charging-state the output of the ZCD sensor is known and equals 2'*b*01. Sampling is performed at the beginning of each system clock cycle, from the turn-off command instance, until discharging-state is commenced, or a change at the ZCD sensor's output is detected.

The second approach, referred to as *asynchronous sampling*, is based on a single-sample at the turn-off instance. The sampling moment is determined based on a delay-estimation-logic which performs initial estimation of the system delay at startup and further tunes to the actual sampling instance during operation. By doing so, at the cost of slightly more complex control hardware, a single sample timing control is enabled. Based on the estimated delay, the asynchronous sampling unit produces a clock-based sampling signal, which is

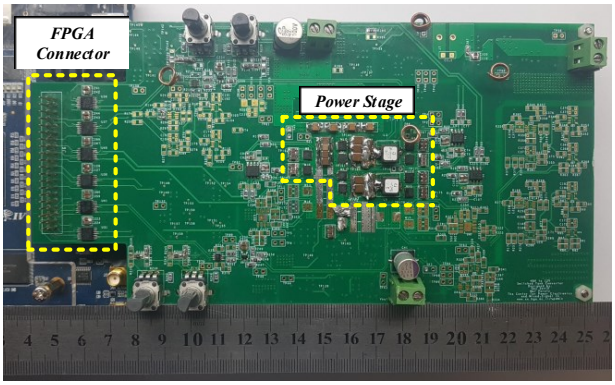

Fig. 6. Photograph of the PCB of 4:1 STC.

TABLE II – EXPERIMENTAL PROTOTYPE VALUES AND PARAMETERS

Component	*Value*
Input voltage V_{in}	48V
Output power	650W
Resonant capacitor C_{r1}, C_{r2}	2.35µF
Resonant inductor L_{r1}, L_{r2}	70nH
Flying capacitor C_f	40µF
Q_1-Q_4	40V/2.5mΩ
Q_5-Q_{10}	25V/1.3mΩ

the input to a delay-line based module, resulting in a sampling signal with a time-resolution of a single delay-element, as shown in Fig. 1.

Regardless of the chosen sampling approach, once closed-loop operation is enabled, the on-time of each sub-circuit is modified independently and the STC switching frequency is set according to (5). The startup value for the on-time of each resonator related sub-circuit is chosen to satisfy the following:

$$0 < T_{on} < 2\pi\sqrt{L_r C_r}\ , \tag{7}$$

so that the resonator current will not change its polarity twice on the course of a charging period, i.e. convergence to ZCS is assured for a wide range of initial switching periods, with up to 100% deviation from the true value.

IV. SIMULATIION AND EXPERIMENTAL VALIDATION

To validate the operation of the 4:1 STC with the self-tuned ZCS control, a 48V-to-12V experimental prototype has been designed, fabricated and tested. The experimental STC hardware has been designed on a 14-layer PCB, shown in Fig. 6, and is rated for 650W with effective power-stage dimensions of 5cmX2cmX0.6cm. The components' parameters and values are detailed in Table II. The self-tuning control scheme, with the two sampling approaches have been implemented on Altera Cyclone IV FPGA using Quartus environment. In addition, several demonstrative cases have been simulated to verify the effectiveness of the control and to enable in-depth examination of the experimental results.

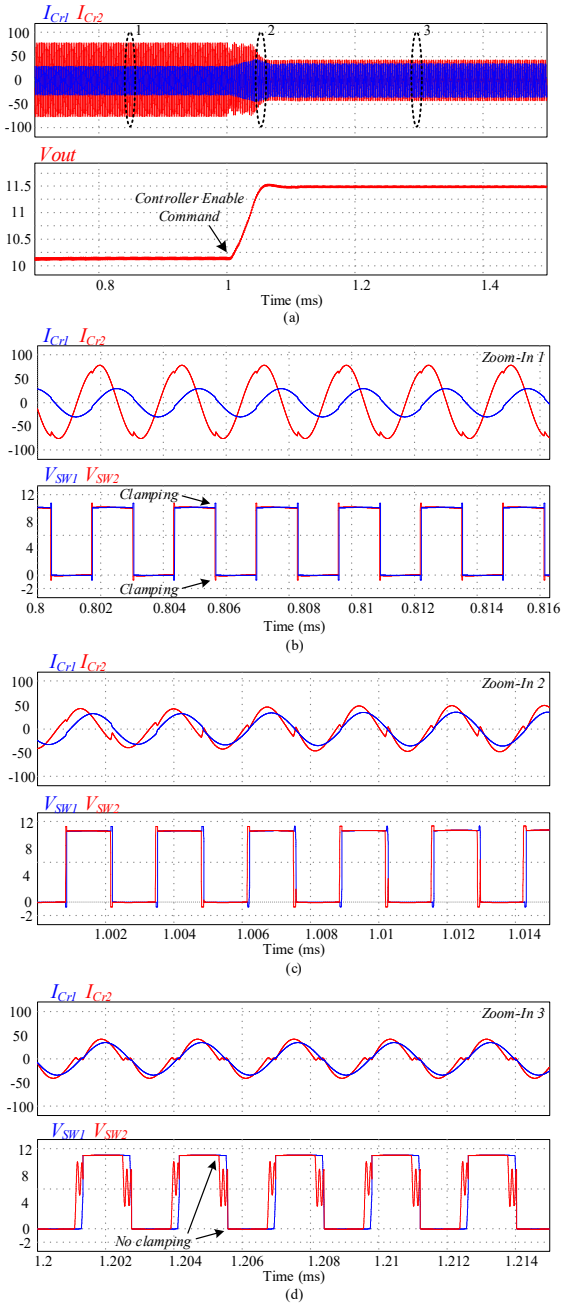

Fig. 7. Convergence to ZCS of a 4:1 STC with mismatched tanks. (a) Resonant currents and output voltage. (b) Zoom-in on the resonant currents and switching nodes in open-loop. (c) Zoom-in on the resonant currents and switching nodes during convergence. (d) Zoom-in on the resonant currents and switching nodes at ZCS.

A. Time-Domain results

The dynamic response of STC with self-tuning control, has been verified by a set of simulations conducted in PSIM (PowerSim, Inc.). Among the simulated cases are convergence to ZCS of matched and mismatched tanks under various operating conditions.

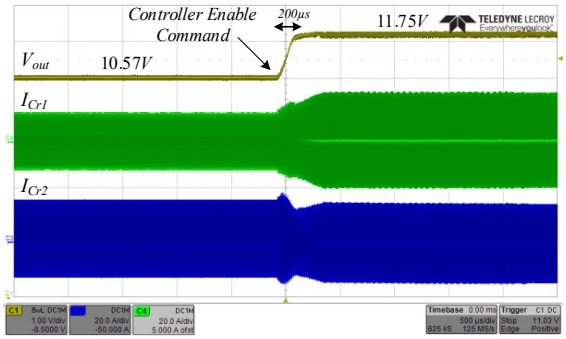

(a)

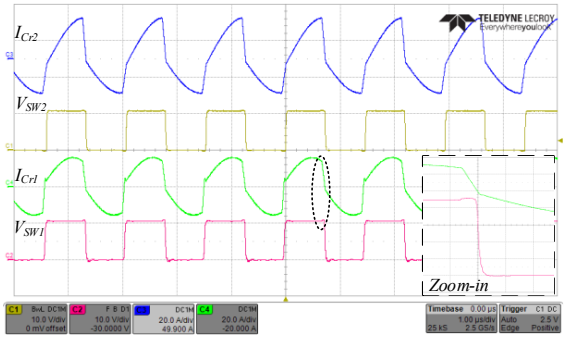

(b)

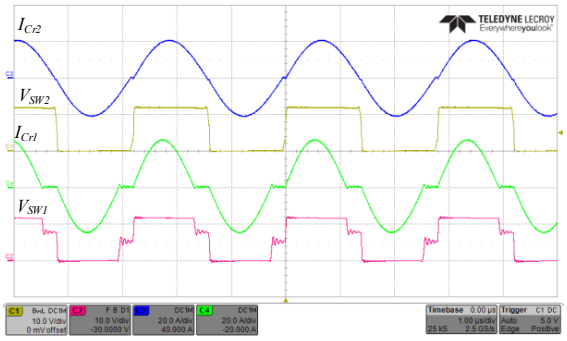

(c)

Fig. 8. Experimental results of a 4:1 STC's transition from open-loop early-switching to ZCS by the self-tuned control. (a) Full view of the tanks' currents and the output voltage. (b) Zoom-in view during open-loop operation of the tanks' currents (top-blue, middle-green) 20A/div, switching nodes (middle-yellow, bottom-red) 10V/div, time scale 1μs/div. (c) Zoom-in view during ZCS self-tuned operation of the tanks' currents (top-blue, middle-green) 20A/div, switching nodes (middle-yellow, bottom-red) 10V/div, time scale 1μs/div.

A simulated case of convergence to ZCS of a STC with mismatched tanks is shown in Fig. 7. The passive components of the resonant tanks were chosen with ±10% variation from their nominal values to verify the effectiveness of the control method under non-ideal operating conditions. The parameters of the nominal values of the passive components are: C_r=2.35μF, L_r=70nH, R_L=0.26Ω. Results of the self-tuning process are shown in Fig. 7a-d, demonstrating convergence onto tuned conditions from off-tune starting points of both resonators. As can be seen, the voltage at the switching nodes is a direct indicator to the switching-state. Once the controller is enabled, the on-time of each resonator is modified according to its resonant period and the switching frequency of the STC

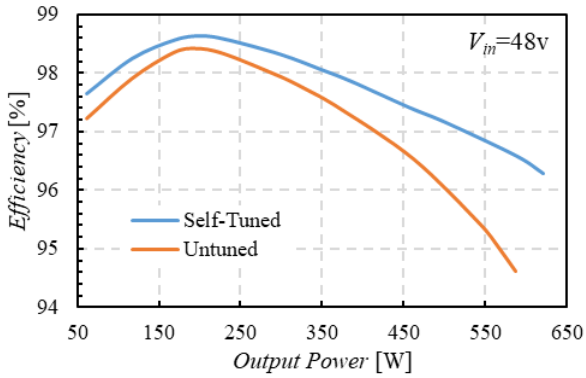

Fig. 9. Efficiency curves of STC with mismatched tanks.

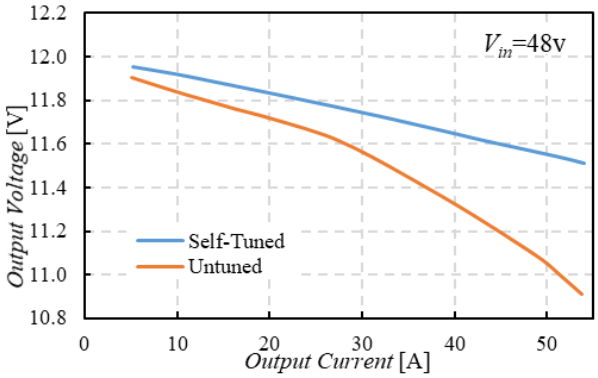

Fig. 10. Output voltage droop measurements of STC with mismatched tanks.

is set accordingly. It can be seen that the output voltage increases to approximately 12V, which is the no-load target voltage, indicating that in the context of optimal charge transfer, the on-time of each resonator has been properly tuned.

Fig. 8 shows experimental waveforms for closed-loop operation with deliberate mismatch between the resonant tanks (C_{r1}=2.62μF, L_{r1}=70nH, C_{r2}=2.35μF, L_{r2}=50nH). In addition, the switching frequency during open-loop operation is arbitrarily chosen to verify convergence to ZCS with no information of the nominal resonant frequency. Fig. 8a shows smooth transition from open-loop early-switching to ZCS of both resonant tanks. A zoomed-in view of the resonant currents as well as the switching nodes is shown in Fig. 8b-c. As can be seen in Fig. 8a, once the tuning process is initiated the output voltage gradually increases from 10.57V to 11.75V, which correlates to the improved charge transfer rate achieved in tuned operation.

B. Efficiency and Thermal Performance

Efficiency curves of the 4:1 STC with mismatched tanks (C_{r1}=2.82μF, L_{r1}=70nH, C_{r2}=2.82μF, L_{r2}=50nH) under untuned and self-tuned conditions are shown in Fig. 9. The STC's efficiency is over 97% for most of the load range and reaches peak efficiency of 98.4% and 98.6% for open-loop and self-tuned conditions, respectively. Output voltage droop measurements, which are shown in Fig. 10, as well as the efficiency curves of Fig. 9 demonstrate the effectiveness of the self-tuned control, in particular for higher loads where rms and core losses are eminent.

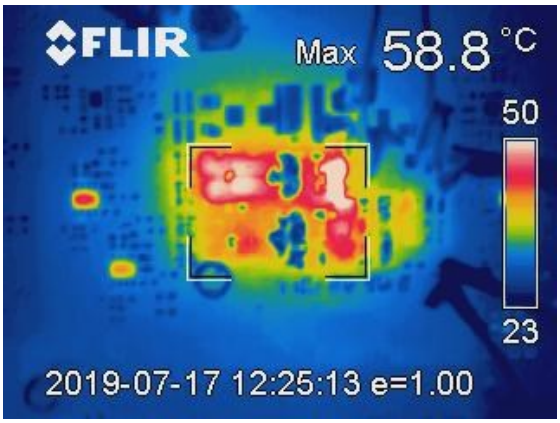

(a)

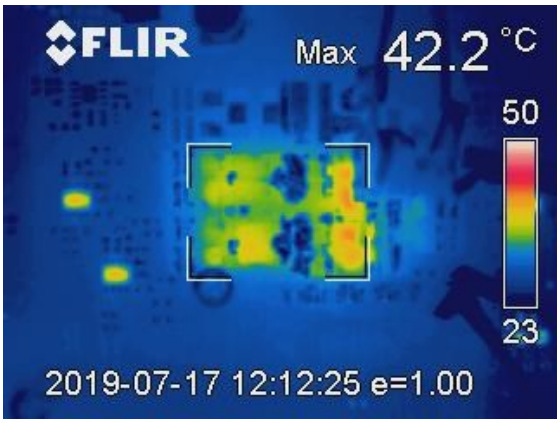

(b)

Fig. 11. Thermal performance of STC with mismatched tanks and output power of 350W. (a) Untuned operation. (b) With self-tuned control.

Mismatched operation also results in an uneven thermal performance due to circulating currents in the system. Thermal images of the power-stage at 350W output power with only fan-cooling, under untuned and self-tuned conditions are shown in Fig. 11a and Fig. 11b, respectively. It can be seen that self-tuned control is crucial not only for increasing efficiency, but also for maintaining even thermal performance of both resonators.

V. Conclusion

An optimal soft-switched self-tuned control for 48V-to-12V STC has been presented. The control modifies the conduction time of each resonator to half of its resonant period, to utilize maximum charge transfer to the load for increased output voltage and efficiency. Evaluation of the resonator's current polarity at turn-off is performed by a simple and cost-effective ZCD sensor. Two approaches have been developed for the sensor's data acquisition, taking into account any delays between the controller's gating command and the actual turn-off of the power-stage transistors. The control operation has been experimentally validated on a 650W 48V-to-12V STC prototype with PCB area of 5cmX2cmX0.6cm, demonstrating peak efficiency of 98.6% at 200W, and accurate on-the-fly tuning capabilities over the entire load range and for various component mismatch scenarios.

Acknowledgment

This research was supported by THE ISRAEL SCIENCE FOUNDATION grant number 2186/19.
This research was supported by Vishay Ltd., Siliconix IC division.

References

[1] M. D. Seeman and S. R. Sanders, "Analysis and Optimization of Switched-Capacitor DC–DC Converters," in *IEEE Transactions on Power Electronics*, vol. 23, no. 2, pp. 841-851, March 2008.

[2] M. N. Gitau and C. L. Kala-Konga, "Multilevel switched-capacitor DC-DC converter with reduced capacitor bank," *IECON 2010 - 36th Annual Conference on IEEE Industrial Electronics Society*, Glendale, AZ, 2010, pp. 576-581.

[3] H. Le, S. R. Sanders and E. Alon, "Design Techniques for Fully Integrated Switched-Capacitor DC-DC Converters," in *IEEE Journal of Solid-State Circuits*, vol. 46, no. 9, pp. 2120-2131, Sept. 2011.

[4] F. Zhang, L. Du, F. Z. Peng and Z. Qian, "A New Design Method for High-Power High-Efficiency Switched-Capacitor DC–DC Converters," in *IEEE Transactions on Power Electronics*, vol. 23, no. 2, pp. 832-840, March 2008.

[5] S. R. Sanders, E. Alon, H. Le, M. D. Seeman, M. John and V. W. Ng, "The Road to Fully Integrated DC–DC Conversion via the Switched-Capacitor Approach," in *IEEE Transactions on Power Electronics*, vol. 28, no. 9, pp. 4146-4155, Sept. 2013.

[6] C. Cheung, S. Tan, C. K. Tse and A. Ioinovici, "On Energy Efficiency of Switched-Capacitor Converters," in *IEEE Transactions on Power Electronics*, vol. 28, no. 2, pp. 862-876, Feb. 2013.

[7] D. Cao and F. Z. Peng, "Zero-Current-Switching Multilevel Modular Switched-Capacitor DC–DC Converter," in *IEEE Transactions on Industry Applications*, vol. 46, no. 6, pp. 2536-2544, Nov.-Dec. 2010.

[8] D. Cao and F. Z. Peng, "A family of zero current switching switched-capacitor dc-dc converters," *2010 Twenty-Fifth Annual IEEE Applied Power Electronics Conference and Exposition (APEC)*, Palm Springs, CA, 2010, pp. 1365-1372.

[9] R. C. N. Pilawa-Podgurski, D. M. Giuliano and D. J. Perreault, "Merged two-stage power converter architecture with soft-charging switched-capacitor energy transfer," *2008 IEEE Power Electronics Specialists Conference*, Rhodes, 2008, pp. 4008-4015.

[10] A. Ioinovici, "Switched-capacitor power electronics circuits," in *IEEE Circuits and Systems Magazine*, vol. 1, no. 3, pp. 37-42, 2001.

[11] G. Wu, X. Ruan and Z. Ye, "Nonisolated High Step-Up DC–DC Converters Adopting Switched-Capacitor Cell," in *IEEE Transactions on Industrial Electronics*, vol. 62, no. 1, pp. 383-393, Jan. 2015.

[12] E. Frachtenberg, "Holistic Datacenter Design in the Open Compute Project," in *Computer*, vol. 45, no. 7, pp. 83-85, July 2012.

[13] O. Jong, Q. Li and F. C. Lee, "Resonant Switched-Capacitor Converter with Multi-Resonant Frequencies," *2019 IEEE Applied Power Electronics Conference and Exposition (APEC)*, Anaheim, CA, USA, 2019, pp. 2177-2184.

[14] H. Setiadi and H. Fujita, "Control and Performance of New Asymmetrical Operation for Switched-Capacitor-based Resonant Converters," *2018 International Power Electronics Conference (IPEC-Niigata 2018 -ECCE Asia)*, Niigata, 2018, pp. 626-631.

[15] K. Sano and H. Fujita, "Improving dynamic performance and efficiency of a resonant switched-capacitor converter based on phase-shift control," *2009 IEEE Energy Conversion Congress and Exposition*, San Jose, CA, 2009, pp. 3509-3515.

[16] S. Jiang, S. Saggini, C. Nan, X. Li, C. Chung and M. Yazdani, "Switched Tank Converters," in *IEEE Transactions on Power Electronics*, vol. 34, no. 6, pp. 5048-5062, June 2019.

[17] Y. Li, X. Lyu, D. Cao, S. Jiang and C. Nan, "A 98.55% Efficiency Switched-Tank Converter for Data Center Application," in *IEEE Transactions on Industry Applications*, vol. 54, no. 6, pp. 6205-6222, Nov.-Dec. 2018.

[18] Infineon (2019, April) "Powering next generation datacenters: Infineon's 48V high-efficiency, two-stage architecture power distribution" [Online].

[19] A. Cervera and M. M. Peretz, "A Family of Switched-Resonant Converters With Wide Conversion Ratio and Controlled Sourcing Features for Volume-Sensitive Applications," in *IEEE Journal of Emerging and Selected Topics in Power Electronics*, vol. 7, no. 2, pp. 910-921, June 2019.

[20] K. K. Law, K. W. E. Cheng and Y. P. B. Yeung, "Design and analysis of switched-capacitor-based step-up resonant converters," in *IEEE Transactions on Circuits and Systems I: Regular Papers*, vol. 52, no. 5, pp. 943-948, May 2005.

[21] Y. Lei and R. C. N. Pilawa-Podgurski, "A General Method for Analyzing Resonant and Soft-Charging Operation of Switched-Capacitor Converters," in *IEEE Transactions on Power Electronics*, vol. 30, no. 10, pp. 5650-5664, Oct. 2015.

[22] E. Hamo, M. Evzelman and M. M. Peretz, "Modeling and Analysis of Resonant Switched-Capacitor Converters With Free-Wheeling ZCS," in *IEEE Transactions on Power Electronics*, vol. 30, no. 9, pp. 4952-4959, Sept. 2015.

[23] E. Hamo, A. Cervera and M. M. Peretz, "Multiple Conversion Ratio Resonant Switched-Capacitor Converter With Active Zero Current Detection," in *IEEE Transactions on Power Electronics*, vol. 30, no. 4, pp. 2073-2083, April 2015.

[24] K. W. E. Cheng, "New generation of switched capacitor converters," *PESC 98 Record. 29th Annual IEEE Power Electronics Specialists Conference (Cat. No.98CH36196)*, Fukuoka, 1998, pp. 1529-1535 vol.2.

[25] J. F. Dickson, "On-chip high-voltage generation in MNOS integrated circuits using an improved voltage multiplier technique," in *IEEE Journal of Solid-State Circuits*, vol. 11, no. 3, pp. 374-378, June 1976.

[26] K. J. Chen *et al*., "GaN-on-Si Power Technology: Devices and Applications," in *IEEE Transactions on Electron Devices*, vol. 64, no. 3, pp. 779-795, March 2017.

[27] G. Loechelt *et al*., "A high-speed silicon FET for efficient DC-DC power conversion," *2012 24th International Symposium on Power Semiconductor Devices and ICs*, Bruges, 2012, pp. 85-88.

[28] H. Chen, B. Ji, V. Pickert and W. Cao, "Real-Time Temperature Estimation for Power MOSFETs Considering Thermal Aging Effects," in *IEEE Transactions on Device and Materials Reliability*, vol. 14, no. 1, pp. 220-228, March 2014.

[29] L. E. Wojewoda, M. J. Hill, K. Radhakrishnan and N. Goyal, "Use Condition Characterization of MLCCs," in *IEEE Transactions on Advanced Packaging*, vol. 32, no. 1, pp. 109-115, Feb. 2009.

[30] S. Ziegler, R. C. Woodward, H. H. Iu and L. J. Borle, "Current Sensing Techniques: A Review," in *IEEE Sensors Journal*, vol. 9, no. 4, pp. 354-376, April 2009.

[31] H. P. Forghani-zadeh and G. A. Rincon-Mora, "Current-sensing techniques for DC-DC converters," *The 2002 45th Midwest Symposium on Circuits and Systems, 2002. MWSCAS-2002.*, Tulsa, OK, USA, 2002, pp. II-II.